Hypersonic Ionizing Air Viscous Shock-Layer Flows over Sphere Cones

E. W. MINER* AND CLARK H. LEWIS†
Virginia Polytechnic Institute and State University, Blacksburg, Va.

Hypersonic, nonequilibrium viscous flow with ionization over nonanalytic blunt bodies is considered. The equations which govern the viscous shock-layer flow are presented and the method by which the equations are solved is discussed. The predictions of the present finite-difference method are compared with other numerical predictions as well as with experimental data. Flows over two sphere cones are considered, the RAM C re-entry body (a 9° sphere cone at 233,000 ft and 25,000 fps) and a 7.5° sphere cone at the experimental wind-tunnel conditions of Pappas and Lee. The predictions of the present method agreed well with the experimental data and with the other numerical predictions except those of Kang and Dunn for the 9° sphere cone. Substantial differences were found between the present predictions and the more approximate predictions of Kang and Dunn for heat-transfer distributions and temperature profiles.

Nomenclature

C_i = concentration of species i, ρ_i/ρ
C_p^* = specific heat at constant pressure
D_i = binary diffusion coefficient, $D_i^*\rho_\infty^*/\mu_{ref}^*$
ECW = denotes equilibrium catalytic wall
FVSL = denotes fully viscous shock layer
h = static enthalpy, h^*/U_∞^{*2}
H = total enthalpy, H^*/U_∞^{*2}
k = thermal conductivity, $k^*/(\mu_{ref}^* C_{p\infty}^*)$
Le_i = Lewis number, $C_p^*\rho^* D_i^*/k^*$
M = molecular weight
$\bar{M}$ = mixture molecular weight, $1/(\sum_i C_i/M_i)$
ns = number of species
NSS = denotes no shock slip
N_e = number of electrons/CM^3
NCW = denotes noncatalytic wall
P = pressure, $P^*/(\rho_\infty^* U_\infty^{*2})$
Pr = Prandtl number, $C_p^*\mu^*/k^*$
q = heat transfer, $q^*/(\rho_\infty^* U_\infty^{*3})$
r = body radius, r^*/R_n^*
R = universal gas constant
R_n^* = body nose radius
Re_s = shock Reynolds number, $\rho_\infty^* U_\infty^* R_n^*/\mu_{sh}^*$
s = coordinate measured along body surface, s^*/R_n^*
s_{tan} = location of sphere-cone tangent point
St = Stanton number, $q_w/(H_\infty - H_w)$
SS = denotes shock slip
T = temperature, T^*/T_{ref}^*
T_{ref}^* = reference temperature, $U_\infty^{*2}/C_{p\infty}^*$
TVSL = denotes thin viscous shock layer
u = velocity component tangent to the body surface, u^*/U_∞^*
v = velocity component normal to the body surface, v^*/U_∞^*
y = coordinate measured normal to the body, y^*/R_n^*
z = coordinate measured along body axis, z^*/R_n^*
ε = Reynolds number parameter, $[\mu_{ref}^*/\rho_\infty^* U_\infty^* R_n^*]^{1/2}$
κ = surface curvature, $\kappa^* R_n^*$
μ = coefficient of viscosity, μ^*/μ_{ref}^*
μ_{ref}^* = coefficient of viscosity evaluated at T_{ref}^*
ρ = density, ρ^*/ρ_∞^*
ϕ = angle between body tangent and axis

Superscripts

j = indicator for axisymmetric flow 1) or two-dimensional flow 0)
$*$ = dimensional quantities

Subscripts

eq = equilibrium value
i = specie i
sh = value behind the shock
w = wall value
o = stagnation point value
∞ = freestream value

Introduction

WHILE supersonic and hypersonic flows over blunt bodies have been of interest in fluid dynamics for many years, recent developments in aerodynamics and space flight have increasingly focused attention on the problem of predicting the blunt body flowfield. In the approach most commonly used, the flowfield over the body is treated in two parts, an inviscid outer flow and a viscous boundary layer. Many methods have been developed for solving the inviscid outer flow, as examples, the methods of Inouye, Rakich, and Lomax[1]; Rizzi and Inouye[2]; and Kutler, Reinhardt, and Warming.[3] Likewise, many methods have been developed for solving the boundary-layer flow; two particular examples are the methods of Blottner and Flugge-Lotz[4] and Blottner.[5]

This approach to the problem generally worked quite well. It is, however, most appropriate for supersonic, high Reynolds number flows. As interest in hypersonic, low Reynolds number flows increased (for example, for reentry applications including the space shuttle), problems were encountered in applying first-order boundary-layer theory to such flows. Some of the problems, such as displacement-thickness interaction, were partially met by using second-order boundary-layer theory, as an example, the work of Lewis.[6] Another problem of the boundary-layer methods is determining the edge conditions. For supersonic, high Reynolds number flows in which the boundary-layer is thin compared to the shock layer thickness and more specifically the entropy layer thickness, it is generally adequate to consider the conditions at the boundary-layer edge to be the same as given by the inviscid solution at the body surface. For hypersonic, low Reynolds number flows in which the boundary layer is not thin, determining the edge conditions for the boundary layer can be most difficult (see, for example, Ref. 6). In the method of Blottner,[5] edge conditions were optionally determined by tracking streamlines from the shock crossing point to the boundary-layer edge or by entropy-layer swallowing.

Many of the problems (including those previously mentioned)

Received January 16, 1974; revision received April 16, 1974.
Index categories: Viscous Nonboundary-Layer Flows; Reactive Flows; Supersonic and Hypersonic Flow.

* Assistant Professor, Aerospace and Ocean Engineering Department; presently curator, Science and Technology Department, National Air and Space Museum, Smithsonian Institute, Washington, D.C. Associate Member AIAA.
† Professor Aerospace and Ocean Engineering Department. Associate Fellow AIAA.

associated with computing viscous, hypersonic flows over blunt bodies can be overcome by the viscous shock-layer approach in which the entire flowfield from the body to the shock is treated in a unified manner. Knowledge of the shock shape is still required (to determine the flow properties behind the shock), but problems such as those of streamline tracking and displacement-thickness interaction are avoided. While many researchers have been involved in developing viscous shock-layer methods, the one who achieved perhaps the greatest degree of success was Davis.[7,8]

An alternative approach to obtaining solutions for hypersonic blunt body flows has been the use of the full Navier-Stokes equations, for example, the method of Jain and Adimurthy.[9,10] Such methods have been quite successful in providing solutions for the stagnation region but generally have been applied only about one nose radius downstream. Further, the elliptic nature of the equations, at least in the physical coordinates, increases the complexity of the solution procedure and restricts the application of the methods in the downstream direction.

The first objective of the present research was to develop a method for predicting hypersonic, low Reynolds number flowfields over nonanalytic blunt bodies. The downstream region was of considerable interest and the method could not be restricted to the stagnation region. A second objective was that the method would not be subject to the problems involved in applying boundary-layer theory to such flows (problems such as displacement-thickness interaction and streamline tracking).

Both objectives were partially met by the viscous shock-layer methods of Davis,[7,8] but his methods were restricted to analytic bodies such as hyperboliods for which the pressure distribution was nearly Newtonian. Despite the restriction to analytic bodies the viscous shock-layer methods of Davis[7,8] had several advantages. The principal equations were parabolic in the streamwise direction, and thus there was no restriction on obtaining downstream solutions. A finite-difference method was used for solving the equations which gave very good accuracy in reasonably short computing times. Further, and quite important, for increasing Reynolds numbers the equations tend to first order boundary-layer equations, and thus the methods were not restricted to only shock-layer flow regimes but could also be applied in the boundary-layer regime as well. In fact, the boundary-layer equations are a subset of the viscous shock-layer equations. Before discussing the present work, the methods of Davis[7,8] are briefly described.

In Ref. 7, Davis developed a set of viscous shock-layer equations for a perfect gas valid from the body to the shock. The equations are accurate to second order in the Reynolds number parameter, ε. In the solution procedure used by Davis, a first global solution was obtained using the thin viscous shock layer (TVSL) assumption and subsequent global iterations were for a fully viscous shock layer (FVSL) or for TVSL. Davis considered only hyperboloids and, for the first (TVSL) global iteration, used the assumption that the shock angle was the same as the body angle. In subsequent global iterations the shock angle was computed from the body angle and the previous global iteration value of the shock-layer thickness derivative. This technique successfully gave the correct shock shape for the analytic bodies Davis considered. In Ref. 8 the governing equations were extended to treat a reacting binary gas mixture.

In the present work, the viscous shock-layer equations which follow the formulation of Davis were solved for flows over sphere-cones. The present method is for nonequilibrium, multicomponent, ionizing air; dissociating oxygen is also included. Predictions of the present method were compared with predictions of perfect gas boundary-layer flow from the method given in Refs. 11 and 12, with predictions of seven-species, nonequilibrium boundary-layer flow using the method described in Refs. 13 and 14, and with the no-injection, experimental data of Pappas and Lee.[15] Predictions of the present method were also compared with the results Kang and Dunn[16-19] obtained with a more approximate integral method. The governing equations used by Kang and Dunn were the first-order boundary-layer equations without the longitudinal pressure gradient term but with the normal momentum equation, which was nonzero only on the spherical portion of the body. Predicted electron concentration profiles were compared with the predicted and experimental profiles given by Evans, Schexnayder, and Huber.[20]

Analysis

In the present work, the governing equations for viscous shock-layer flows follow the formulation of Davis[7,8] in that the equations apply to axisymmetric or two-dimensional flows and are accurate to second order in terms of the Reynolds number parameter, ε, from the body to the shock. Both longitudinal and transverse curvature are included. As given by Davis, the governing viscous shock-layer equations were specialized for a perfect gas[7] or a binary, reacting mixture of oxygen atoms and molecules.[8] In the present work the governing equations are for a multicomponent mixture of reacting gases and are given below.

Continuity Equation:

$$\frac{\partial}{\partial s}[\rho u(r+y\cos\phi)^j] + \frac{\partial}{\partial y}[(1+\kappa y)(r+y\cos\phi)^j \rho v] = 0 \tag{1}$$

S Momentum Equation:

$$\frac{1}{1+\kappa y}\rho u\frac{\partial u}{\partial s} + \rho v\frac{\partial u}{\partial y} + \rho uv\frac{\kappa}{1+\kappa y} + \frac{1}{1+\kappa y}\frac{\partial P}{\partial s} = \varepsilon^2\frac{\partial}{\partial y}\left[\mu\left(\frac{\partial u}{\partial y} - \frac{\kappa u}{1+\kappa y}\right)\right] + \varepsilon^2\left(\frac{2\kappa}{1+\kappa y} + \frac{j\cos\phi}{r+y\cos\phi}\right)\times\left[\mu\left(\frac{\partial u}{\partial y} - \frac{\kappa u}{1+\kappa y}\right)\right] \tag{2}$$

Y Momentum Equation:

$$\text{FVSL}\quad \frac{\partial P}{\partial y} = \rho\left[\frac{\kappa u^2}{1+\kappa y} - \frac{u}{1+\kappa y}\frac{\partial v}{\partial s} + v\frac{\partial v}{\partial y}\right] \tag{3a}$$

$$\text{TVSL}\quad \frac{\partial P}{\partial y} = \frac{1}{1+\kappa y}\rho\kappa u^2 \tag{3b}$$

Energy Equation:

$$\frac{1}{1+\kappa y}\rho u\frac{\partial H}{\partial s} + \rho v\frac{\partial H}{\partial y} - v\frac{\partial P}{\partial y} + \frac{\rho\kappa u^2 v}{1+\kappa y} = \varepsilon^2\frac{\partial}{\partial y}\left[\frac{\mu}{Pr}\frac{\partial H}{\partial y} + \frac{\mu}{Pr}\sum_{i=1}^{ns} h_i(Le_i-1)\frac{\partial C_i}{\partial y} + \frac{\mu}{Pr}(Pr-1)u\frac{\partial u}{\partial y} - \frac{\mu\kappa u^2}{1+\kappa y}\right] + \varepsilon^2\left(\frac{\kappa}{1+\kappa y} + \frac{j\cos\phi}{r+y\cos\phi}\right)\times\left[\frac{\mu}{Pr}\frac{\partial H}{\partial y} + \frac{\mu}{Pr}\sum_{i=1}^{ns} h_i(Le_i-1)\frac{\partial C_i}{\partial y} + \frac{\mu}{Pr}(Pr-1)u\frac{\partial u}{\partial y} - \frac{\mu\kappa u^2}{1+\kappa y}\right] \tag{4}$$

Species Conservation Equation:

$$\frac{1}{1+\kappa y}\rho u\frac{\partial C_i}{\partial s} + \rho v\frac{\partial C_i}{\partial y} = \varepsilon^2\frac{\partial}{\partial y}\left(\rho D_i\frac{\partial C_i}{\partial y}\right) + \dot{W}_i + \varepsilon^2\left(\frac{\kappa}{1+\kappa y} + \frac{j\cos\phi}{r+y\cos\phi}\right)\left(\rho D_i\frac{\partial C_i}{\partial y}\right) \tag{5}$$

The coordinate system for the equations is shown in Fig. 1.

In addition to the governing conservation equations, the equation of state is needed:

$$P = \rho RT/\bar{M}C_{p\infty}{}^* \tag{6}$$

Boundary conditions are also required. At the body surface the boundary conditions are $u = 0$, $v = 0$, $T = T_w$, and $C_i = C_{i_{eq}}(T_w)$ for the equilibrium catalytic wall (ECW) condition or $\partial C_i/\partial y = 0$ if the surface is noncatalytic (NCW). In the present work the surface temperatures were sufficiently low that the ECW condition could be approximated by a fully catalytic surface. Without shock slip (NSS) the edge conditions are $u = u_{sh}$, $v = v_{sh}$, $T = T_{sh}$ and $C_i = C_{i\infty}$. With shock slip (SS) (for the perfect or binary gases) the edge conditions are the shock slip conditions given by Davis.[7,8]

To simplify the solution procedure, the equations were normalized by the variable values behind the shock as was done

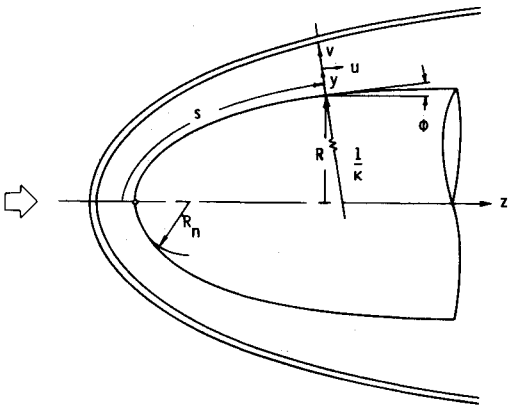

Fig. 1 Coordinate system for viscous shock layer flow over blunt bodies.

by Davis.[7,8] With the normalized equations, the same spacing of the finite-difference grid in the normal direction could be used over the entire body. The normalized s momentum, energy, and species conservation equations were of the same standard parabolic form as given by Davis[7] and were solved by the same marching integration technique. At each s location the equations were solved in the order of species, energy, s momentum, continuity, and y momentum. The integration of the continuity equation determined both the v profile and the shock-layer thickness, y_{sh}. At each location the solution was iterated until convergence was obtained for the velocity, temperature, and species concentration profiles at all points in the finite-difference grid. After a global iteration was completed (i.e., a solution obtained for the entire length of the body), shock angle and shock slope data were updated from a smoothed, weighted average of the shock-layer thickness distribution and another global iteration was made. For the two cases considered in the present paper, the emphasis was on the viscous shock-layer method and the advantages which it provided. There were some differences between TVSL and FVSL results near the stagnation point but downstream these differences were quite small. Computing times were less for TVSL and thus most of the present results were for TVSL. For calculations for TVSL, two global iterations were normally made; for the calculations for FVSL, three global iterations were normally made.

In the present work, the method which Davis[7,8] used for determining the shock angle for the first global iteration could not be applied. Since Davis considered only hyperboloids, he made the assumption for the first global iteration that the shock and body angle were the same and then, in the second iteration, the shock angle was determined from the shock-layer thickness computed in the first global iteration. This procedure worked well for analytic bodies such as hyperboloids but could not be used for nonanalytic bodies such as sphere cones. In the present work for sphere cones, an initial shock shape was determined from a blunt body, method of characteristics procedure such as that of Inouye, Rakich, and Lomax.[1] This shock shape was used for the first global iteration and was then updated for subsequent global iterations. In both the present work and that of Davis,[7,8] an FVSL solution must be preceeded by a TVSL solution since the FVSL solution used the v profiles from the previous global iteration.

The way in which the body curvature, κ, is treated in the present work also differs from the work of Davis.[7,8] For the hyperboloids Davis considered, the curvature is a continuous, monotonic function. For a spherically blunted cone, however, κ is discontinuous at the sphere-cone tangent point. To provide a continuous distribution of curvature, an approximate value of κ was computed in the present work from the expression

$$\kappa = 1 - \{1 + \exp[-f(s - s_{\tan})]\}^{-1} \tag{7}$$

where f is a constant with a typical value of 5. Calculations were made with other values of f, and also for κ discontinuous. The results of these calculations showed that the effects of changing the value of f were mostly confined to the region $s = s_{\tan} \pm 1$ and that little effect was observed for $s > 4$ or 5 or for $s < 0.5$.

In the present work viscosity, thermal conductivity, and reaction rate data for the binary gas viscous shock-layer predictions were the same as used by Davis,[8] while the thermodynamic data were from Browne.[21,22] For the multi-component gas, boundary-layer predictions, transport, and rate data were those given by Blottner,[24] and the thermodynamic data were from Browne.[21-23] For the multicomponent, viscous shock-layer predictions, the transport data were from Blottner,[24] the thermodynamic data from Browne,[21-23] and the reaction rate data were matched with those of Evans, Schexnayder, and Huber[20] or with those of Kang and Dunn.[17]

After a solution was obtained, wall-measurable quantities were calculated. In the present work an area of interest was heat transfer to the body surface. In terms of the nondimensional variables, the heat transfer is given by

$$q_w = -\varepsilon^2 \left[k \frac{\partial T}{\partial y} + \sum_{i=1}^{ns} h_i D_i \frac{\partial C_i}{\partial y} \right]_{y=0} \tag{8}$$

Results and Discussion

In the present work, the principal interest was in viscous shock-layer flows over sphere cones, but some predictions were made for flows over hyperboloids. Since for analytic bodies such as hyperboloids, the present method is almost identical to that of Davis,[7,8] predictions of the present method for hyperboloids should agree almost exactly with the results of Davis.[8] While the results are not presented, such was indeed the case for the 10° half-angle hyperboloid at 225,000 ft (Davis[8]). For this case the Reynolds number parameter was $\varepsilon = 0.197$ and the Reynolds number values were $Re_\infty/\text{ft} = 8355$, $Re_\infty/R_n = 690$, and $Re_s = 63.7$. Other cases considered by Davis[8] were from 100 kft to 250 kft with $Re_s = 9555$ to 23.7. The agreement of the present predictions with the predictions of Davis[8] for flow over a hyperboloid for this case should indicate the accuracy of present technique.

In the present paper, predictions for two cases are presented as representative of the application of the present viscous shock-layer method to flows over sphere cones. The values of Re_s for these cases were 270 and 193 and while low, were still high enough for boundary-layer theory to give reasonable results. Further, for each case, some experimental data were available as were predictions made using finite-difference boundary-layer methods of well-established accuracy. The first case corresponded to the 230,000 ft alt point on the trajectory of the RAM C re-entry body (a 9° sphere cone with $R_n = 6$ in. at 25,000 fps). The second case considered in the present paper was the 7.5° sphere cone ($R_n = 1$ in. at $M_\infty = 13.4$) investigated by Pappas and Lee[15] in their experiments.

RAM C Re-Entry Case

The RAM C flights were part of a program conducted by the NASA Langley Research Center for studying flowfield electron concentrations under re-entry conditions. The body for each RAM C flight was a 9° sphere cone with a 6 in. nose radius. Associated with the experimental program were theoretical studies using numerical methods. For example, Kang and Dunn[16-19] used a TVSL integral method procedure to predict electron concentration profiles for several points on the RAM C trajectory. Also included in Refs. 16–19 were other flowfield quantities such as temperature profiles and surface heat-transfer distributions.

The results presented by Kang and Dunn were for the higher alt points on the RAM C trajectory where viscous shock-layer theory would be more appropriate. Predictions of the RAM C electron concentrations have also been made by other researchers. For example, Evans, Schexnayder, and Huber[20,25] applied two different boundary-layer methods and obtained

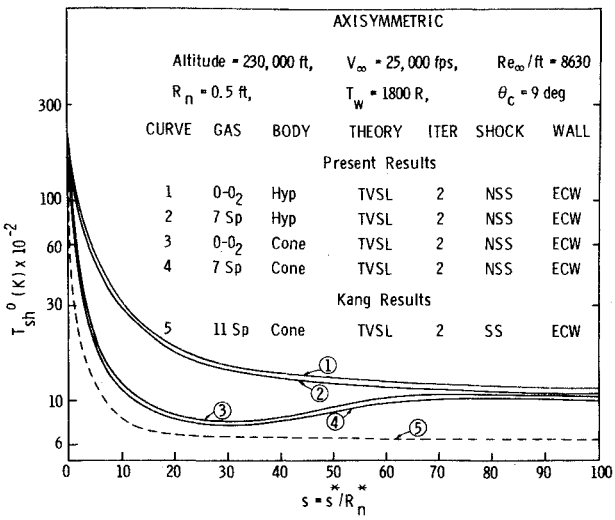

Fig. 2 Shock-temperature distributions for RAM C conditions.

reasonable agreement with the experimental data with both methods. The use of the boundary-layer approach limited Evans et al. to consideration of the lower altitude points of the RAM C trajectory. However, the 230 kft point was considered by Evans et al. and by Kang and Dunn. For the 230,000 ft alt point, predictions of the present finite-difference, viscous shock-layer method were compared with the predictions of a finite-difference, boundary-layer method (Evans, Schexnayder, and Huber[20]) and the predictions of the TVSL integral method of Kang and Dunn.[16-19] In the present work the principal emphasis *was not on predicting electron concentrations* but rather was on predicting the hypersonic, viscous flowfield over spherically blunted cones with electron concentrations a part of the flowfield predictions. The present results included viscous shock-layer predictions for three gas models (perfect gas, dissociating oxygen, and multicomponent, ionizing air). Also included were results of the inviscid, perfect gas method of Inouye, Rakich, and Lomax,[1] a perfect gas, boundary-layer method[11,12] and a seven species, nonequilibrium, ionizing air boundary-layer method.[13,14] Some predictions for flow over a 9° half-angle hyperboloid were included in addition to the predictions for the 9° sphere cone.

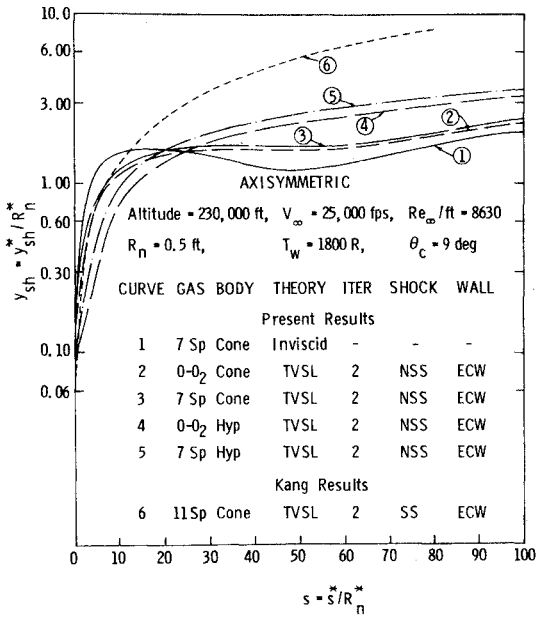

Fig. 3 Shock-layer thickness distributions for 9 sphere cone, RAM C conditions.

One reason for choosing the RAM C conditions at 230 kft was experimental data and other numerical results were available for this case. Kang and Dunn[16-19] presented results for distributions of Stanton number, temperature behind the shock and shock-layer thickness in addition to temperature and electron concentration profiles. The experimental data and the numerical results of Evans, Schexnayder, and Huber[20] were for electron concentration profiles only. The differences between the present predictions and the numerical results of Kang and Dunn[16-19] were unexpectedly large. Most of the discussion of the differences between the present results and the results of Kang and Dunn will be deferred to the end of this section.

Distributions of temperature behind the shock are shown in Fig. 2 for the RAM C sphere cone and a 9° half-angle hyperboloid. Although the end of RAM C body was at $s = 9.2$ the results given by Kang and Dunn went to $s = 90$ and the present predictions were extended to $s = 100$. At the stagnation point there were small differences in T_{sh} due to differences in the gas model, but the sphere-cone and hyperboloid gave the same value for the same gas model. The differences in T_{sh} due to differences in gas model for the present results were greatest at the stagnation point and decreased as the shock became more oblique. In the downstream portion of the flow, the principal differences in T_{sh} were due to the differences in the bodies. The present results showed the expected differences in T_{sh} distributions for hyperboloids and sphere-cones and correctly predicted the distributions of T_{sh} coming together at $s \simeq 80$. In contrast to the present results, Kang and Dunn obtained a quite different distribution of T_{sh}.

Distributions of shock-layer thickness are compared in Fig. 3. While the present results show some distinct differences, they were in substantial agreement, especially for $s > 20$. The principal differences in the present results were again due to the differences in the bodies considered. The present shock-layer predictions showed only small differences in y_{sh} due to the chemistry. For the sphere-cone, the viscous shock-layer results were in reasonable agreement with the inviscid results but did not show as sharp a decrease in y_{sh} between $s = 15$ and 40. The present

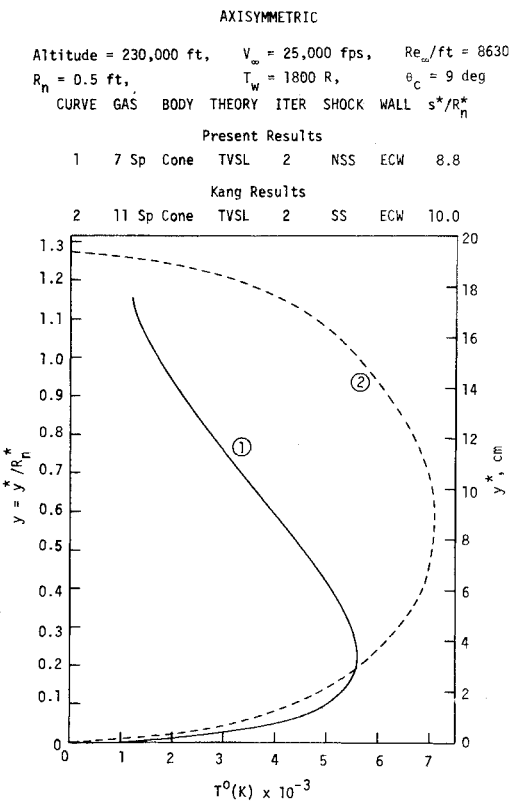

Fig. 4 Temperature profiles near probe location, RAM C conditions.

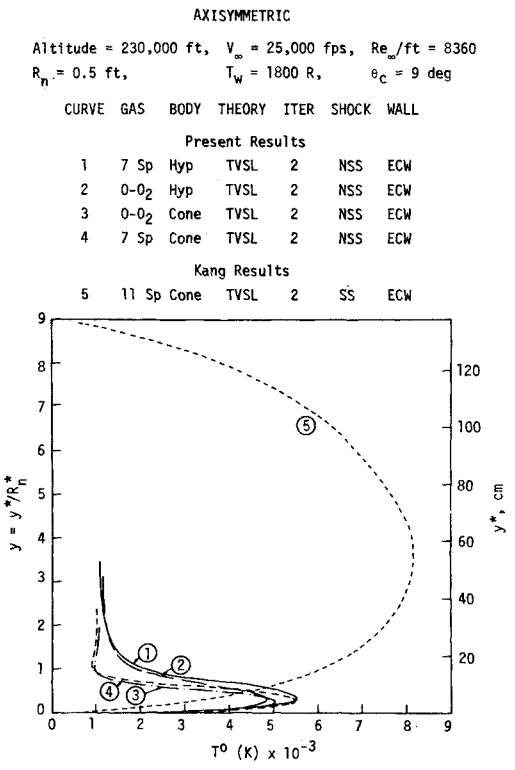

Fig. 5 Temperature profiles for 9° sphere cone at $s/R_n = 90$, RAM C conditions.

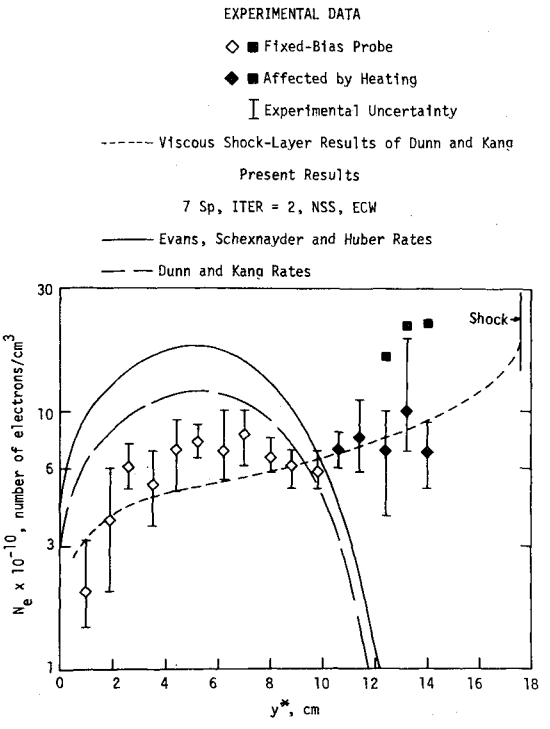

Fig. 7 Present electron concentration profiles with different reaction rates compared with experimental and Kang and Dunn profiles, $s/R_n = 8.8$, RAM C conditions.

results for the hyperboloid were lower than the sphere-cone results for $s < 20$ but were about 50% greater for $s > 50$.

Temperature profiles are shown in Figs. 4 and 5. The profiles in Fig. 4 were for the probe location. The present method profile was for $s = 8.8$, the probe location. The profile of Kang and Dunn (for $s = 10$) was the profile closest to the probe location which they gave (the next closest profiles were for $s = 3.0$ and 20.0). The profiles in Fig. 5 were for $s = 90$. The profiles for the hyperboloid showed a smoother transition from the outer flow to an inner, viscous flow than did the present sphere-cone profiles. The profiles for dissociating oxygen showed a 10% lower peak temperature than did the profiles for ionizing air. Despite these small differences, the four present profiles showed a very distinct inner viscous region ($y/y_{sh} = 0.0$ to 0.5) and an outer inviscid region ($y/y_{sh} = 0.5$ to 1.0). While not shown, the velocity profiles also indicated the edge of the viscous layer at $y/y_{sh} \simeq 0.5$. The present viscous shock-layer temperature profiles have also been compared (not shown here) with the temperature profiles predicted by the seven species boundary-layer method[13,14] for flow over the 9° sphere cone. The boundary-layer and viscous shock-layer profiles showed differences in peak and edge temperatures but were quite similar in character and the boundary-layer profiles also indicated the edge of the viscous layer at $y \simeq 1.0$ as did the viscous shock-layer profiles. Further, a comparison of the present profiles, as shown in Figs. 4 and 5, clearly showed the distinct downstream development of an outer inviscid flow and an inner viscous flow.

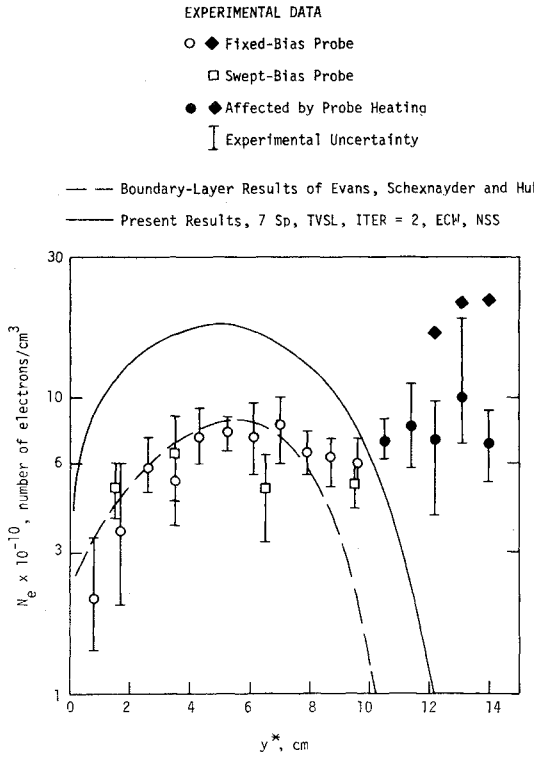

Fig. 6 Present electron concentration profiles compared with experimental and boundary-layer theory profiles, $s/R_n = 8.8$, RAM C conditions.

Electron concentration profiles for the RAM C at 230 kft are shown in Figs. 6 and 7. The data that the present results are compared with were taken from figures in Ref. 20. In Fig. 6, the present results are compared with the experimental data and the results Evans, Schexnayder, and Huber[20] obtained with a very reliable finite-difference, boundary-layer method. The reaction rate constants used for the present results in Fig. 6 were matched to those of Ref. 20. The present results agreed reasonably well with the experimental data and with the boundary-layer theory results of Ref. 20 as to level of ionization and quite well with the boundary-layer theory results as to character of the N_e profile. The present viscous shock-layer theory predicted a higher temperature in the viscous layer than did the boundary-layer theory of Ref. 20, and this difference accounted for most of the difference in the N_e profiles.

Predictions of electron concentrations were also influenced by the reaction rates used. Predictions were made for the RAM C

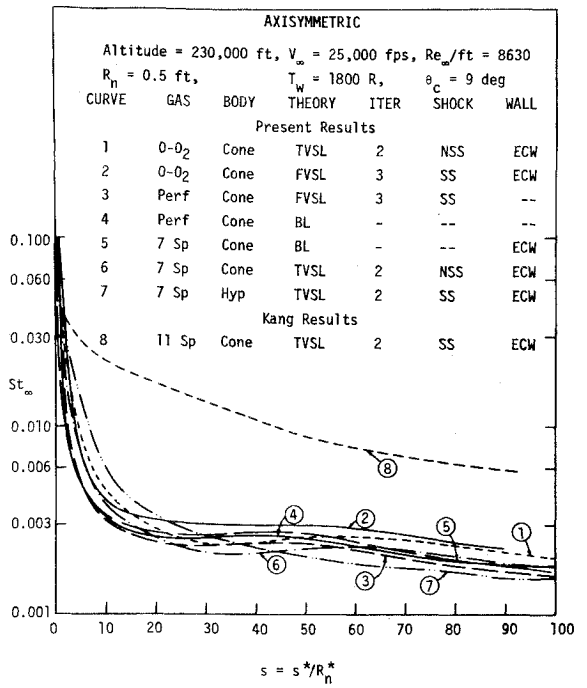

Fig. 8 Stanton number distributions for 9° sphere cone, RAM C conditions.

case using reaction rate constants matched to those of Kang and Dunn.[17] The profiles predicted using the two different sets of rate constants are compared in Fig. 7. The principal difference was a one-third reduction in peak N_e using Ref. 17 rate constants. The experimental data and the TVSL results of Kang and Dunn[17] were taken from Ref. 20. Except for the experimental data between $y = 10$ and 14 cm, which were affected by probe heating,[20] the use of the Ref. 17 reaction rate constants improved the agreement between the predictions of the present method and the experimental data. The results of Kang and Dunn[17] also agreed well with the experimental data, at least for $y < 10$ cm. However, as noted by Evans, Schexnayder, and Huber,[20] the experimental data did not support the upswing in N_e near the shock that the Kang and Dunn[17] results gave. The present results also did not show such an upswing, but rather showed the opposite trend.

Heat-transfer distributions are shown in Fig. 8. The present results include boundary-layer (perfect gas[11,12] and seven species nonequilibrium air[13,14]) and viscous shock-layer (perfect gas, dissociating oxygen, and seven species nonequilibrium air) predictions for the RAM C9° sphere cone and seven species TVSL predictions for a 9° half-angle hyperboloid. All of the present results were in good agreement for this case. Some differences due to chemistry and geometry did exist, but the agreement was good despite the diversity of methods, chemistry, and geometry.

The heat-transfer rates at the stagnation point are not clearly shown in Fig. 8 but are given in Table 1. The present results for TVSL, seven species, 1st iteration were obtained using the method of Ref. 14. The present results showed some distinct differences but agreed reasonably well, at least compared with the results of Kang.

In the preceding discussion, the differences between the present results and the results of Kang and Dunn[16-19] were only briefly mentioned. In Refs. 16–19 a large number of results were presented but comparisons were made with no other numerical results and the only experimental results with which comparisons were made were for electron concentration profiles. As mentioned above, their results apparently agreed well with the N_e profiles but as Evans, Schexnayder, and Huber[20] noted the experimental data did not support the upswing in the N_e profile near the shock as obtained by Kang and Dunn. It was also observed in Ref. 20 that the method of Kang and Dunn overpredicted the N_e values measured by the microwave reflectometers on the RAM C-II at the more forward body stations ($s \simeq 0.8$ and 2.1) by factors as large as 20; whereas for 233 kft and lower, the results of the boundary-layer theory used in Ref. 20 agreed with the reflectometer data at all body stations. These two notes from Ref. 20 raise questions about the results given in Refs. 16–19. Further questions must be raised by the differences between the results from Refs. 16–19 and the present results.

As mentioned above the emphasis of the present work was on predicting the hypersonic viscous flowfield over spherically blunted cones with electron concentration profiles only a part of the flowfield predictions. Since electron concentration profiles are subject to changes in reaction rate constants as well as changes in temperature profiles, mean flowfield quantities such as heat-transfer distributions would be a more reliable measure of method accuracy. Since there were no experimental data for y_{sh} or St distributions, calculations were made using well-known, well-established, independent methods (inviscid flowfield technique of Ref. 1 and boundary-layer flows from Refs. 11–14). The predictions of the present viscous shock-layer methods agreed well with the results of these independent methods. In contrast, there were large differences between the present predictions and the results of Kang and Dunn.[16-19]

The value of T_{sh} at $s = 0$ obtained by Kang and Dunn as shown in Fig. 2 was nearly the same as for the present results, but for $s > 1$ their values of T_{sh} were distinctly lower than the present T_{sh} values. For $s > 80$ their value of T_{sh} was only about 60% of the present values. The distributions of T_{sh} obtained by Kang and Dunn should imply a lower shock angle (for $s > 5$ or 10) than that in the present results. The shock-layer thickness distributions shown in Fig. 3 seem to clearly indicate that (for $s > 10$) the shock angle obtained by Kang and Dunn was considerably greater than that in the present results. In fact, at $s \simeq 10$ the values of y_{sh} were all approximately unity, but at $s = 90$ the present results gave $y_{sh} \simeq 1.9$ for the inviscid flow over the sphere-cone, $y_{sh} \simeq 2.2$ for the sphere-cone shock-layer flows and $y_{sh} \simeq 3.5$ for the hyperboloid shock-layer flows; whereas Kang and Dunn's results gave $y_{sh} \simeq 9$. Thus, the trends of the T_{sh} and y_{sh} distributions from Refs. 16–19 were distinctly contradictory and inconsistent.

The temperature profiles as shown in Figs. 4 and 5 also differed markedly. The profiles of Kang and Dunn were nearly the same shape at $s = 10$ as at $s = 90$, while the present profiles showed a strong downstream influence. The present profiles showed a distinct outer inviscid region, somewhat weak at $s = 8.8$ but quite clear at $s = 90$. The present profiles showed about the same peak value of T at $s = 8.8$ and 90. In the profiles from Refs. 16–19, the peak value increased from $T \simeq 7200°K$ at $s = 10$ to $T \simeq 8200°K$ at $s = 90$.

With the temperature profiles as different as shown in Fig. 4, differences in electron concentration profiles were expected, but not the differences shown by the profiles in Fig. 7. The present results gave a peak value of N_e at $y \simeq 5$ cm while the peak of

Table 1 Stagnation heat-transfer for sphere-cone, 230,000 ft conditions

Model	Gas	Iter	Wall	Shock	$\dot{q}$, BTU/ft^2—sec
			Present Results		
BL	PG	...	...	...	231.074
BL	7 sp	...	ECW	...	177.250
FVSL	PG	3	...	SS	123.973
FVSL	O–O_2	3	ECW	SS	238.742
TVSL	O–O_2	2	ECW	NSS	190.278
TVSL	7 sp	2	ECW	NSS	156.883
TVSL	7 sp	1	ECW	SS	252.539
			Kang Results		
TVSL	11 sp	...	ECW	SS	87.772

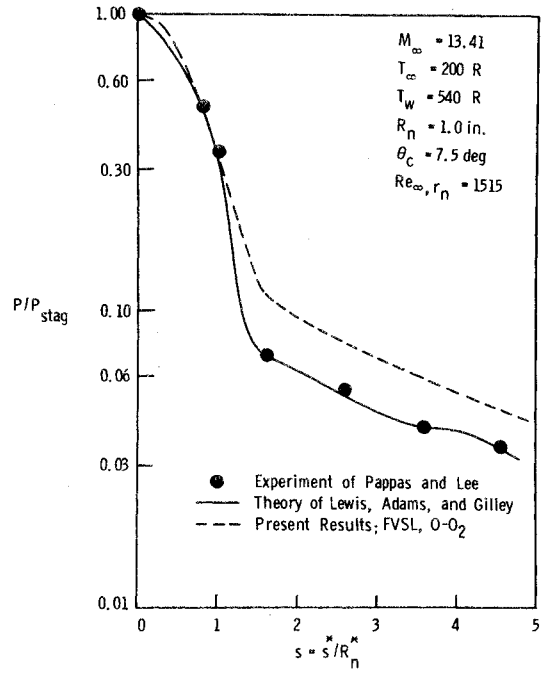

Fig. 9 Normalized surface-pressure distributions for sphere cone, Ames conditions.

the temperature profile was at $y \simeq 3.5$ cm, but T at $y = 5$ cm was only slightly lower than T at $y = 3.5$ cm. This was quite reasonable, but in the results of Kang and Dunn, the peak value of N_e was at the shock ($y \simeq 17$ cm) while the peak value of T was at $y \simeq 9$ cm. Further, T at the shock, where the peak in N_e occurred, was less than one eighth the peak temperature. Also, while the N_e profile of Kang and Dunn apparently agreed well with the experimental data, the peak value of N_e was two or three times the peak of the experimental data (points affected by probe heating excluded), twice the peak of the present results and three times the peak obtained by Evans, Schexnayder, and Huber.[20]

At the stagnation point, the heat transfer obtained by Kang and Dunn was one-half to one-third that predicted by the finite-difference methods used in the present work (see Table 1).

In contrast to the stagnation point results, over most of the conical portion of the body the heat transfer predicted by Kang and Dunn was two to six times that predicted by the boundary-layer and viscous shock-layer methods used in the present work. However, the temperature profiles shown in Figs. 4 and 5 would apparently indicate that the heat transfer obtained by Kang and Dunn should have been lower than the present results.

Ames Experimental Case

Comparisons have also been made with some hypersonic wind tunnel data of Pappas and Lee[15] at the NASA Ames Research Center. In the experimental program, surface pressure and heat-transfer distributions were measured over a 7.5° sphere-cone at Mach 13 with varying rates of injection of foreign gases. Included in the experimental data were distributions for the no injection case. Experimental and present predictions of pressure and heat-transfer distributions are shown in Fig. 9 and 10. Also shown in these figures is the previous first-order boundary-layer theory of Lewis, Adams, and Gilley[13] including transverse curvature and displacement-thickness interaction for the Ames conditions. The results from Ref. 13 were obtained using a global iteration for determining the displacement-thickness interaction effects, and the inviscid body pressure for the effective body was obtained using a blunt-body method of characteristics procedure similar to that of Ref. 1. The present theory did not compare as well with the experimental data as did the previous boundary-layer theory with viscous interaction included. In the present viscous shock-layer method, the effect of the discontinuity in surface curvature, κ, was most distinct immediately upstream of the sphere-cone tangent point and for a short distance downstream. The sphere cone considered by Pappas and Lee[15] ended at $s \simeq 5$, and almost all of this body was within the length affected by the discontinuity in κ. Despite the effect of the discontinuity in κ, the agreement between the experimental data and the predictions of the present viscous shock-layer theory was quite good.

While the RAM C conditions were quite different from the Ames conditions, the Reynolds numbers were of the same order ($Re_\infty/R_n = 4315$ for the RAM C conditions and $Re_\infty/R_n = 1515$ for the Ames conditions). The shock Reynolds numbers were also similar (RAM C, $Re_s = 269$; Ames, $Re_s = 193$) and the values of the Reynolds number parameter were nearly the same (RAM C, $\varepsilon = 0.0965$; Ames, $\varepsilon = 0.0980$). The Reynolds number similarity between the two cases should allow comparison of the normalized heat-transfer distributions. The left portion of Fig. 11 shows the same data as Fig. 10 but with the present results for the RAM C conditions added. The present predictions for the RAM C and Ames conditions were in quite good agreement even though there was a difference in cone angle (and thus in the location of the sphere-cone tangent points). Further, the present viscous shock-layer results for the RAM C conditions agreed well with the Ames experimental data. The results of Kang and Dunn[16-19] for the RAM C are not shown in the left portion of Fig. 11 but are shown in the right part of the figure in which data from Fig. 8 are presented again in normalized form. The right part of Fig. 11 clearly shows that for $s > 3$ the results of Kang and Dunn were higher by an order of magnitude or more than the present results. A comparison of the results of Kang and Dunn for the RAM C with the Ames experimental data would show a difference by a factor of 11 or 12 at $s = 4$ or 4.5. The values of Re_∞/R_n and Re_s given above indicate that the Ames conditions were at least as much in a viscous shock-layer regime as the RAM C conditions and it is most surprising that the trend of the results of Kang and Dunn[16-19] would not have agreed better with the experimental data of Pappas and Lee.[15]

Computing Time Required

Some of the computing times required for the RAM C conditions are given in Table 2. These computing times were

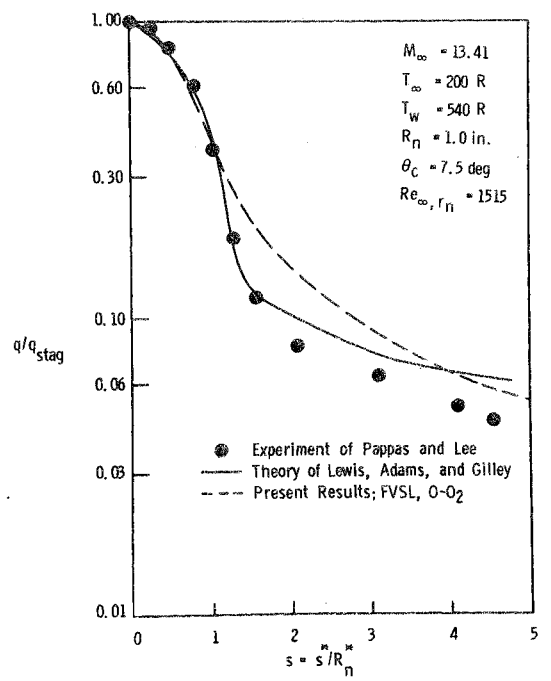

Fig. 10 Normalized heat-transfer distributions for sphere cone, Ames conditions.

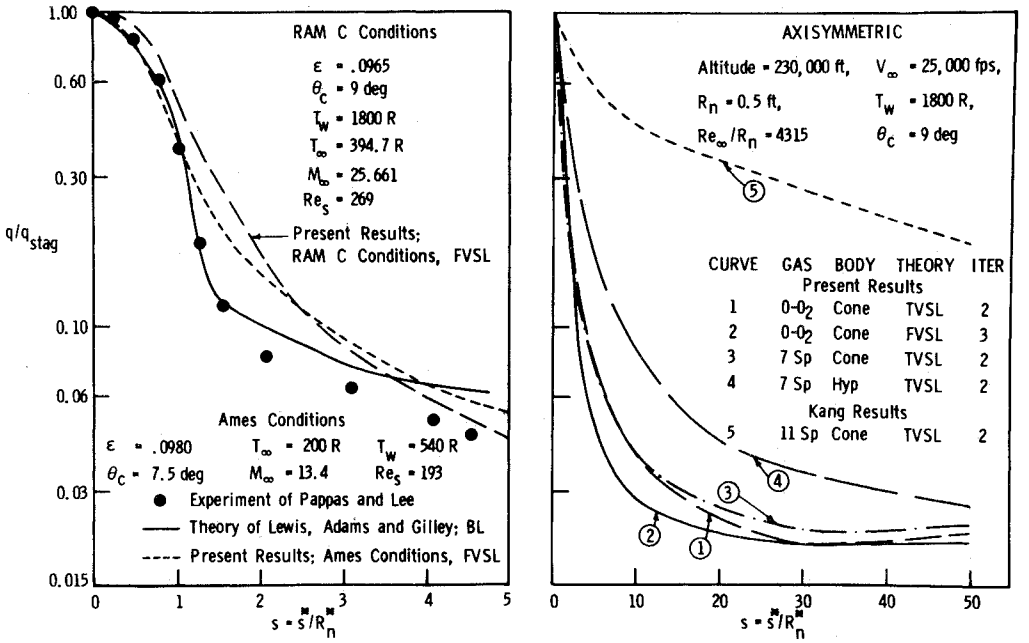

Fig. 11 Comparison of predicted heat-transfer distributions for sphere cone, RAM C and Ames conditions.

obtained on the IBM 370/158 system of the Computing Center of the Virginia Polytechnic Institute and State University. The inviscid gas model calculation used the blunt-body method of characteristics technique of Ref. 1. The PG boundary-layer (BL) calculation was made with the method of Refs. 11 and 12. The viscous shock-layer (VSL) computing times were for the present method. The inviscid method generated the pressure distribution for the BL calculation and the initial shock shape for the VSL calculations. In the VSL method, the first global iteration was for O–O_2 and subsequent global iterations were for either O–O_2 or the 7 sp gas model.

The computing time (not shown) for a PG VSL was nearly the same as for the PG BL. As shown, a global iteration for the O–O_2 VSL required about twice the computing time of the PG BL. For O–O_2, if the second global iteration was TVSL, the computing time was almost the same as for the first global iteration. If, however, the second iteration was FVSL, the second iteration required three times the computing time of the first iteration when the same value of N was used, and twice the computing time when the step size restriction was relaxed.

For the 7 sp gas model, the step size restriction was relaxed. The TVSL global iteration required six times the computing time required for O–O_2, and for the FVSL global iteration, the computing time was 3.5 to 5 times that required for the O–O_2 global iteration.

Table 2 Computing times for RAM C sphere cone to $s/R_n = 120$[a]

Global Iteration Number[b]	Gas Model	Viscous Model	No. of Stations	No. of Iterations[c]	N[d]	Computing Time[e] Min:sec
...	PG	Inviscid	...	...	...	5:35
...	PG	BL	61	189	3	1:34
1st	O–O_2	TVSL	52	271	3	3:29
2nd	O–O_2	TVSL	58	291	3	3:34
2nd	O–O_2	FVSL	100	715	3	10:00
2nd	O–O_2	FVSL	62	474	4	6:58
2nd	7 sp	TVSL	42	241	4	20:40
2nd	7 sp	FVSL	57	415	4	35:45

[a] Convergence test of 1% for velocity, temperature and species profiles at each grid point.
[b] Data are for the indicated global iteration only.
[c] Total number of station iterations for the global iteration.
[d] The s step size was doubled if a converged solution was obtained with the number of station iterations $\leq N$.
[e] Execution time; IBM 370/158.

These computing times show that if the differences between the results for TVSL and FVSL are not great, a significant amount of computing time can be saved by using the TVSL model. Further, unless the 7 sp model is required, the computing time can be greatly reduced by using the O–O_2 gas model.

Conclusions

The results of the present finite-difference method for predicting hypersonic viscous shock-layer flows over nonanalytic blunt bodies were compared with predictions of other finite-difference methods and with experimental data. The comparisons showed that the present method reasonably predicted mean flowfield quantities such as temperature profiles, surface heat-transfer distributions, and electron concentration profiles. Also, the trends of the shock temperature and shock layer thickness distributions were quite consistent. The temperature profiles showed the proper downstream development. Further, the predicted peak of the electron concentration profile occurred near the peak of the temperature profile and agreed very well with the peak of the experimental electron concentration profile.

The comparison of the present results with the results of Kang and Dunn indicated that the more approximate integral method of Kang and Dunn is not appropriate for predicting hypersonic viscous shock-layer flows over spherically blunted cones. Even though they obtained apparently good agreement with the RAM C electron concentration profiles, this agreement in fact was not as good it would first appear. Also their results for shock temperature and shock-layer thickness distributions appeared distinctly inconsistent and contradictory. Further, the present prediction of the heat-transfer distributions for the RAM C conditions agreed well with the Ames experimental data, as indeed the Reynolds number similarity would require, but the heat-transfer distribution predicted by the integral method of Kang and Dunn for the RAM C conditions would have differed from the Ames experimental data by an order of magnitude or more on the conical portion of the body.

References

[1] Inouye, M., Rakich, J., and Lomax, H., "A Description of Numerical Methods and Computer Programs for Two-Dimensional and Axisymmetric Supersonic Flow over Blunt Nosed and Flared Bodies," TN D-2970, Aug. 1965, NASA.

[2] Rizzi, A. W. and Inouye, M., "A Time-Split Finite-Volume Technique for Three-Dimensional Blunt-Body Flow," *AIAA Journal*, Vol. 11, No. 11, Nov. 1973, pp. 1478–1485.

[3] Kutler, P., Reinhardt, W. A., and Warming, R. F., "Multishocked, Three-Dimensional Supersonic Flowfields with Real Gas Effects," *AIAA Journal*, Vol. 11, No. 5, May 1973, pp. 657–664.

[4] Blottner, F. G. and Flugge-Lotz, I., "Finite Difference Computation of the Boundary-Layer with Displacement Thickness Interaction," *Journal de Mechanique*, Vol. 11, No. 4, 1964.

[5] Blottner, F. G., "Finite Difference Methods of Solution of the Boundary-Layer Equations," *AIAA Journal*, Vol. 8, No. 2, Feb. 1970, pp. 193–206.

[6] Lewis, C. H., "First Order Treatment of Higher-Order Boundary-Layer Effects," *The Physics of Fluids*, Vol. 13, No. 12, Dec. 1970, pp. 2939–2949.

[7] Davis, R. T., "Numerical Solution of the Hypersonic Viscous Shock-Layer Equations," *AIAA Journal*, Vol. 8, No. 5, May 1970, pp. 843–851.

[8] Davis, R. T., "Hypersonic Flow of a Chemically Reacting Binary Mixture Past a Blunt Body," AIAA Paper 70-805, Los Angeles, Calif., 1970.

[9] Jain, A. C. and Adimurthy, V., "Hypersonic Merged Stagnation Shock Layers, Part I: Adiabatic Wall Case," *AIAA Journal*, Vol. 12, No. 3, March 1974, pp. 342–347.

[10] Jain, A. C. and Adimurthy, V., "Hypersonic Merged Stagnation Shock Layers, Part II: Cold Wall Case," *AIAA Journal*, Vol. 12, No. 3, March 1974, pp. 348–354.

[11] Anderson, E. C. and Lewis, C. H., "Laminar or Turbulent Boundary-Layer Flows of Perfect Gases or Reacting Gas Mixtures in Chemical Equilibrium," CR-1893, 1971, NASA.

[12] Lewis, C. H., Anderson, E. C., and Miner, E. W., "Nonreacting and Chemically Reacting Turbulent Boundary-Layer Flows," AIAA Paper 71-597, Palo Alto, Calif., 1971; also *International Journal for Numerical Methods in Engineering*, Vol. 17, 1973, pp. 3–15.

[13] Lewis, C. H., Adams, J. C., and Gilley, G. E., "Effects of Mass Transfer and Chemical Nonequilibrium on Slender Blunted Cone Pressure and Heat Transfer Distributions at $M_\infty = 13.2$," TR-68-214, Dec. 1968, Arnold Engineering Development Center, Tullahoma, Tenn.

[14] Lewis, C. H. and Miner, E. W., "Stagnation Point Viscous Layers with Mass Transfer," *Computers and Fluids*, Vol. 2, No. 2, Aug. 1974, pp. 117–143.

[15] Pappas, C. C. and Lee, G., "Heat Transfer and Pressure on a Hypersonic Blunt Cone with Mass Addition," *AIAA Journal*, Vol. 8, No. 5, May 1970, pp. 954–956.

[16] Kang, S.-W. and Dunn, M. G., "Hypersonic Viscous Shock Layer with Chemical Nonequilibrium for Spherically Blunted Cones," *AIAA Journal*, Vol. 10, No. 10, Oct. 1972, pp. 1361–1362.

[17] Kang, S.-W., Jones, W. L., and Dunn, M. G., "Theoretical and Measured Electron-Density Distributions at High Altitudes," *AIAA Journal*, Vol. 11, No. 2, Feb. 1973, pp. 141–149.

[18] Kang, S.-W. and Dunn, M. G., "Hypersonic Viscous Shock Layer with Chemical Nonequilibrium for Spherically Blunted Cones," TR-AF-3093-A-1, Feb. 1972, Cornell Aeronautical Lab., Ithaca, N.Y.

[19] Dunn, M. G. and Kang, S.-W., "Theoretical and Experimental Studies of Reentry Plasmas," CR-2232, April 1973, NASA.

[20] Evans, J. S., Schexnayder, C. J., Jr., and Huber, P. W., "Boundary-Layer Electron Profiles for Entry of a Blunt Slender Body at High Altitudes," TN D-7332, July 1973, NASA.

[21] Browne, W. G., "Thermodynamic Properties of Some Atoms and Atomic Ions," MSD Engineering Physics TM2, General Electric Co., Philadelphia, Pa.

[22] Browne, W. G., "Thermodynamic Properties of Some Diatomic and Linear Polyatomic Molecules," MSD Engineering Physics TM3, General Electric Co., Philadelphia, Pa.

[23] Browne, W. G., "Thermodynamic Properties of Some Diatoms and Diatomic Ions at High Temperature," MSD Advanced Aerospace Physics TM8, May 1962, General Electric Co., Philadelphia, Pa.

[24] Blottner, F. G., "Non-Equilibrium Laminar Boundary Layer Flow of Ionized Air," Rept. R64SD56, Nov. 1964, General Electric Co., Philadelphia, Pa.

[25] Huber, P. W., Evans, J. S., and Schexnayder, C. J., Jr., "Comparison of Theoretical and Flight-Measured Ionization in a Blunt Body Re-Entry Flowfield," *AIAA Journal*, Vol. 9, No. 6, June 1971, pp. 1154–1162.

JANUARY 1975 AIAA JOURNAL VOL. 13, NO. 1

Buoyant Convection in Radiating Horizontal Fluid Layers

S. C. TRAUGOTT* AND S. H. YAMAMURA†
Martin Marietta Laboratories, Baltimore, Md.

Buoyancy-driven, two-dimensional convection in a horizontal layer of radiating fluid, confined between isothermal no-slip surfaces, is calculated with a numerical finite difference method. The radiation model was taken to be the grey Milne-Eddington approximation, and the formulation includes quite general radiative boundary conditions. Radiation is found to inhibit convection primarily due to increased stability. For the same ratio of Grashof to critical Grashof numbers, the flowfields are very similar with and without radiation. Convective heat flux can decrease the radiative flux below its static values. The radiative model employed resulted in essentially the same computing time both with and without radiation.

I. Introduction

BUOYANCY-driven convection occurs in horizontal fluid layers in a wide variety of situations. In many of these the characteristic length transverse to the layer, in the direction of gravity, is very much less than the distance along the layer. In such a geometry the thermal drive is related to the density variation across the layer, in contrast to situations in which the forcing is due to imposed horizontal gradients of density or temperature. There is then a stability problem, in addition to the question of the nature of the flow, once buoyant forcing is sufficient to overcome the inhibiting action of friction and heat conduction.

In many instances it is clear that radiative heat transfer also plays a role in the process. Such is the case with stellar convection, convection in a planetary atmosphere, and in laboratory experiments with certain fluids (carbon tetrachloride, ammonia). The role of radiative transfer in modifying critical conditions for the onset of convection has been the subject of considerable

Presented as Paper 74-9 at the AIAA 12th Aerospace Sciences Meeting, Washington, D.C., January 30–February 1, 1974; submitted February 15, 1974, revision received July 22, 1974. Work partially supported by the U.S. Air Force Office of Scientific Research (AFSC), under Contract F44620-71-C-0011.

Index categories: Radiatively Coupled Flows and Heat Transfer; Radiation and Radiative Heat Transfer.

* Principal Research Scientist, Mechanics Department. Associate Fellow AIAA.

† Senior Research Assistant, Mechanics Department.